New regime of inverse saturable absorption for self-stabilizing passively mode-locked lasers

Author(s):
Grange, R.; Haiml, M.; Paschotta, R.; Spuhler, G.J.; Krainer, L.; Golling, M.; Ostinelli, O.; Keller, U.

R. GRANGE[1],✉
M. HAIML[1]
R. PASCHOTTA[1]
G.J. SPÜHLER[1]
L. KRAINER[1]
M. GOLLING[1]
O. OSTINELLI[2,3]
U. KELLER[1]

New regime of inverse saturable absorption for self-stabilizing passively mode-locked lasers

[1] Institute of Quantum Electronics, Physics Department, Swiss Federal Institute of Technology (ETH),
ETH Zürich Hönggerberg, Wolfgang-Pauli-Str. 16, 8093 Zürich, Switzerland
[2] Avalon Photonics, Badenerstrasse 569, P.O. Box, 8048 Zürich, Switzerland
[3] FIRST Center for Micro- and Nanoscience, Swiss Federal Institute of Technology (ETH),
ETH Zürich Hönggerberg, Wolfgang-Pauli-Str. 10, 8093 Zürich, Switzerland

ABSTRACT The reflectivity of a semiconductor saturable absorber mirror (SESAM) is generally expected to increase with increasing pulse energy. However, for higher pulse energies the reflectivity can decrease again; we call this a 'roll-over' of the nonlinear reflectivity curve caused by inverse saturable absorption. We show for several SESAMs that the measured roll-over is consistent with two-photon absorption only for short (femtosecond) pulses, while a stronger (yet unidentified) kind of nonlinear absorption is dominant for longer (picosecond) pulses. These inverse saturable absorption effects have important technological consequences, e.g. for the Q-switching dynamics of passively mode-locked lasers. A simple equation using only measurable SESAM parameters and including inverse saturable absorption is derived for the Q-switched mode-locking threshold. We present various data and discuss the sometimes detrimental effects of this roll-over for femtosecond high repetition rate lasers, as well as the potentially very useful consequences for passively mode-locked multi-GHz lasers. We also discuss strategies to enhance or reduce this induced absorption by using different SESAM designs or semiconductor materials.

PACS 42.60.Fc; 42.70.Nq; 78.20.Ci

1 Introduction

Since 1992, semiconductor saturable absorber mirrors (SESAMs) have been used with great success for self-starting passive continuous-wave mode locking of various types of solid-state lasers [1–4]. A technological key point is to avoid Q-switching instabilities [5], which can be provoked as an unwanted side effect of using a saturable absorber in a laser cavity. Especially for lasers with high pulse repetition rates [6, 7] or high average output powers [8], the tendency for Q-switched mode locking (QML), which is typically observed below a certain threshold for the intracavity power, is a crucial limiting factor. Often it is difficult to achieve a low enough QML threshold.

Theoretical results for the QML threshold [5] have generally been found to be in good agreement with experimental

values. However, particularly for some recent high repetition rate lasers, the QML threshold was found to be significantly lower than expected. Recently, it was shown that for some Er:Yb:glass lasers this could be explained with modified saturation characteristics of the SESAMs used, namely with a roll-over of the nonlinear reflectivity for higher pulse fluences [9].

Two-photon absorption (TPA) has been widely used for optical power limiter [10]. And it has long been known that TPA causes a roll-over in the nonlinear reflectivity which lowers the Q-switching threshold [11, 12]. However, for picosecond pulse durations as in the mentioned Er:Yb:glass lasers this effect would be too weak to be significant for practical values of the pulse fluence. Therefore, it was surprising that a significant roll-over was observed even in this regime [9], while many earlier experiments on other SESAM-mode-locked lasers did not provide evidence for this effect. Note that the need to suppress Q-switching instabilities has enforced the use of SESAMs with reduced modulation depth (maximum nonlinear reflectivity change) of below 1%, particularly in the context of lasers with multi-GHz repetition rates [7]. For such low modulation depths, small induced nonlinear absorption effects acquire importance that always had been covered by the stronger saturable absorption in earlier SESAMs with modulation depth well above 1%. Another important fact is that only recently we managed to raise the accuracy of nonlinear reflectivity measurements on SESAMs [13] to the level that is required to clearly see weak roll-over effects.

In this paper we report precise nonlinear reflectivity measurements of several SESAMs in a wide range of pulse durations between 190 fs and 20 ps. We have found that the observed strong roll-over for femtosecond pulses is consistent with theoretical expectations based on two-photon absorption. For picosecond pulses the roll-over is weaker than for femtosecond pulses but still much stronger than expected from two-photon absorption only. We conclude that an additional mechanism must be at work here, such as free-carrier absorption, Auger recombination, hot-carrier generation, or lattice heating.

In this paper we also discuss the technological consequences of this roll-over, which can be detrimental in some cases (in particular for the generation of very short pulses) but very helpful in other cases. In particular, we find that the unexpectedly strong roll-over for picosecond pulses explains

✉ Fax: +41-1-633-1059, E-mail: grange@phys.ethz.ch

why it was possible to achieve stable operation of passively mode-locked Er:Yb:glass lasers with pulse-repetition rates up to 50 GHz [6], which should be hardly possible without this effect.

We also discuss ways to optimize the amount of TPA for certain applications by changing the thickness of a semiconductor layer [14] or its material composition.

The paper is organized as follows. In Sect. 2, we derive SESAM nonlinear reflectivity equations including TPA for small modulations. Then, in Sect. 3, we present the experimental results with three different pulse durations of the laser sources fitted with the equations obtained in Sect. 2. The beneficial and detrimental effects of the roll-over as well as the issue of the QML threshold with derivation of a simplified condition are discussed in Sect. 4. Section 5 addresses the optimization of the roll-over for different applications, using design and material parameters.

2   Calculation of nonlinear reflectivity with two-photon absorption

A standard SESAM design consists of a distributed Bragg reflector (DBR), a spacer layer, an absorber layer, and a cap layer, as shown in Fig. 1. Due to the small thickness of the quantum-well absorber, the additional absorption caused by TPA almost only occurs in the spacer layer, in the DBR layers, and possibly in a thicker cap layer, but only to a negligible amount in the absorber layer. Moreover, the entire nonlinear absorption of a few percent has little effect on the field distribution, which therefore can simply be calculated without TPA. For stronger nonlinear absorption, we would have to take into account that the absorption caused by TPA depends on the optical field distribution, which itself is modified by the saturable and inverse saturable absorption, so that the exact calculation becomes complicated.

For weak nonlinear absorption and for a given incident intensity I_{inc}, we can then calculate the intensity absorbed by TPA, I_{abs}, by simply integrating:
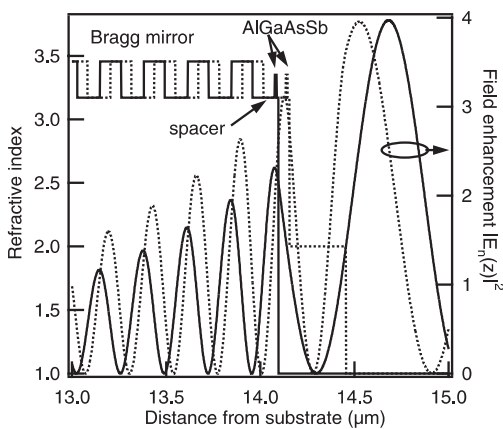
$$I_{\text{abs}} = \int \beta(z) I^2(z) \, dz, \tag{1}$$

FIGURE 1   Standing wave pattern in the as-grown AlGaAsSb SESAM (*solid line*) and the coated SESAM (*dashed line*). The field enhancement $|E_{\text{n}}(z)|^2$ in the absorber is 2.30 for the as-grown SESAM and 3.03 for the coated one

where z is the depth in the structure and $\beta(z)$ is the local TPA coefficient that depends on the material in the structure. The local intensity $I(z)$ is calculated from the normalized electric field $|E_{\text{n}}(z)|^2$ (normalized so that the incident beam would have $|E_{\text{n}}(z)|^2 = 1$) plotted in Fig. 1:

$$I(z) = \frac{c_0 \varepsilon_0}{2} n(z) \, |E(z)|^2 = n(z) \, |E_{\text{n}}(z)|^2 \, I_{\text{inc}}. \tag{2}$$

Here, c_0 is the vacuum speed of light, ε_0 is the dielectric constant, and $n(z)$ is the local refractive index. We then have the relative power loss q_{TPA} caused by TPA:

$$q_{\text{TPA}} = I_{\text{abs}}/I_{\text{inc}}. \tag{3}$$

This is based on the argument that the absorbed power must be missing in the reflected beam, as long as no significant power is transmitted through the substrate. We actually work with pulses of fluence F_{p} and FWHM pulse duration τ_{p}, so that we have to integrate the TPA effect over the temporal shape:

$$q_{\text{TPA}} = \frac{\int I_{\text{abs}}(t) \, dt}{\int I_{\text{inc}}(t) \, dt} = \frac{\int \beta(z) \, n^2(z) \, \left(|E_{\text{n}}(z)|^2\right)^2 dz \int I_{\text{inc}}^2(t) dt}{F_{\text{p}}}. \tag{4}$$

For sech^2-shaped pulses we have

$$\int_{-\infty}^{+\infty} I_{\text{inc}}^2(t) \, dt \approx 0.585 \frac{F_{\text{p}}^2}{\tau_{\text{p}}}. \tag{5}$$

This means that the averaged TPA effect is about 0.585 times the effect for a top-hat pulse with the same fluence and duration. Thus, we obtain

$$q_{\text{TPA}} = 0.585 \frac{F_{\text{p}}}{\tau_{\text{p}}} \int \beta(z) \, n^2(z) \, \left(|E_{\text{n}}(z)|^2\right)^2 dz. \tag{6}$$

Without the roll-over effect, the simplest model for a saturable absorber leads to an intensity absorption coefficient that is reduced from the initial value q_0 to the value $q_0 \exp(-F_{\text{p}}/F_{\text{sat,A}})$ after the passage of a pulse with incident fluence F_{p}. Here, $F_{\text{sat,A}}$ is the saturation fluence of the absorber. The SESAM reflectivity averaged over a whole pulse with fluence F_{p} can then be calculated [5] in the approximation for weak absorption ($q_0 \approx \Delta R$):

$$R(F_{\text{p}}) = R_{\text{ns}} - (1 - \exp(-F_{\text{p}}/F_{\text{sat}})) \frac{\Delta R}{F_{\text{p}}/F_{\text{sat}}} - \frac{F_{\text{p}}}{F_2}, \tag{7}$$

where F_{sat} is the saturation fluence, R_{ns} accounts for nonsaturable losses in the structure [15], ΔR is the modulation depth, and F_2 is the inverse slope of the induced absorption effect (TPA) [13]:

$$F_2 = \frac{\tau_{\text{p}}}{0.585 \int \beta(z) \, n^2(z) \, \left(|E_{\text{n}}(z)|^2\right)^2 dz}. \tag{8}$$

Equation (7) results from a simple absorber model and the assumption of a flat-top spatial beam profile and small modulation; the equations for higher modulations and Gaussian spatial profiles can be derived [13] but are significantly more
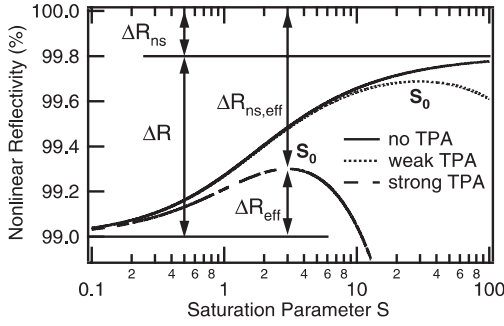
FIGURE 2   Calculated nonlinear reflectivity vs. the saturation parameter S assuming $\Delta R = 0.8\%$ and $\Delta R_{ns} = 0.2\%$ for strong, weak, and no TPA

complicated. In Fig. 2, we display three typical nonlinear reflectivity curves vs. the saturation parameter S, defined as

$$S = \frac{F_p}{F_{sat}}. \tag{9}$$

The modulation depth ΔR is kept constant at 0.8%, and the nonsaturable losses ΔR_{ns} from the absorber layer are assumed to be 0.2% for this example. We defined a pulse fluence F_0 where the reflectivity is maximum, and its corresponding saturation parameter $S_0 = F_0/F_{sat}$. Two examples for weak TPA ($S_0 = 30$) and strong TPA ($S_0 = 3$) are shown in Fig. 2. Obviously, the maximum reflectivity of 99.8% cannot be reached when TPA is present. The reduced effective modulation depth ΔR_{eff} and the effective nonsaturable losses $\Delta R_{ns,eff}$ due to TPA are defined according to Fig. 2.

The pulse fluence for maximum modulation F_0 can be calculated from (7) by

$$\left. \frac{dR(F_p)}{dF_p} \right|_{F_p = S_0 F_{sat}} = 0. \tag{10}$$

For weak TPA ($F_0 > 5 F_{sat}$) when $\exp(-F_p/F_{sat}) \to 0$, we obtain

$$F_0 = \sqrt{F_2 F_{sat} \Delta R} \quad \text{(valid for } F_0 > 5 F_{sat}) \tag{11}$$

or

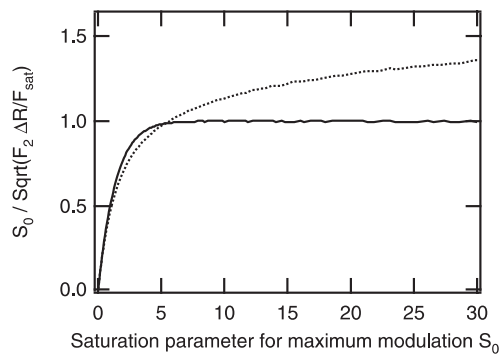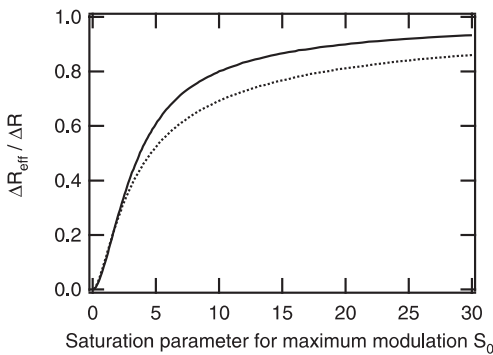$$S_0 = \sqrt{\frac{F_2 \Delta R}{F_{sat}}} \quad \text{(valid for } S_0 > 5). \tag{12}$$

The effective modulation depths ΔR_{eff} and $\Delta R_{ns,eff}$ can then be calculated from $R(S_0)$. Figure 3 shows ΔR_{eff} normalized to ΔR vs. S_0. Accordingly, the effective nonsaturable losses $\Delta R_{ns,eff}$ increase with decreasing ΔR_{eff}; see Figs. 2 and 3. The solid line in Fig. 3 is for a spatial flat-top beam profile. The dashed line is calculated using a Gaussian beam profile [13]. The right-hand graph of Fig. 3 shows the actual (numerically calculated) S_0 relative to the approximation $\sqrt{F_2 \Delta R/F_{sat}}$ vs. S_0, demonstrating the validity of the approximation (12) for $S_0 > 5$.

As the effective modulation depth is strongly reduced for very short pulses, the roll-over limits the usefulness for generation of short pulses. The point where the roll-over prevents any initial reflectivity increase is reached for

$$\left. \frac{dR(F_p)}{dF_p} \right|_{F_p=0} = 0. \tag{13}$$

We use a Taylor expansion for $R(F_p)$ at $F_p = 0$:

$$R(F_p) = R_{ns} - \left(1 - \frac{1}{2}(F_p/F_{sat})\right) \Delta R - \frac{F_p}{F_2}, \tag{14}$$

which leads to the minimal F_2 (strongest induced absorption) given by (13)

$$F_2^{min} = \frac{2 F_{sat}}{\Delta R}. \tag{15}$$

Equation (15) allows for calculating a lower limit for the shortest possible pulses to be obtained with a given SESAM in a mode-locked laser, if we know (e.g. by measurements) the dependence of F_2 on the pulse duration. For TPA, this dependence would simply be linear.

3   Experimental data for nonlinear reflectivity

We measured the nonlinear reflectivity of 1.5-µm SESAMs, based on AlGaAsSb absorbers on InGaAsP/InP DBRs grown by metal–organic vapor-phase epitaxy (MOVPE) on a (100) InP substrate [16, 17]. The designs for the as-grown sample (solid lines) and for a sample with a dielectric coating (dotted lines) are shown in Fig. 1. A 300-nm SiN$_x$ dielectric coating was applied to increase the field-enhancement factor $|E_n|^2$ in the AlGaAsSb absorber from 2.3 (as-grown SESAM) to 3.03 (coated SESAM).

The method and setup to measure the nonlinear reflectivity are completely described in [13]. We use two different types

FIGURE 3   *Left*: effective modulation depth ΔR_{eff} normalized to ΔR vs. the saturation parameter for maximum modulation S_0. *Solid line*: flat-top spatial beam profile. *Dashed line*: Gaussian beam profile. *Right*: numerically calculated S_0 in units of $\sqrt{F_2 \Delta R/F_{sat}}$ vs. S_0, demonstrating the validity of this approximation for $S_0 > 5$

		Measured			Calculated
	Pulse duration	F_{sat} (μJ/cm^2)	ΔR (%)	F_2 (mJ/cm^2)	F_2 (mJ/cm^2)
As-grown SESAM	20 ps	34	1.5	89	400
	3.1 ps	38	1.8	24	63
	190 fs	–	–	3.3	3.8
Coated SESAM	20 ps	24	2.0	54	200
	3.1 ps	22	2.4	15	31
	190 fs	–	–	2.7	1.9

TABLE 1 Measured saturation fluence F_{sat}, modulation depth ΔR, roll-over parameter F_2, and calculated roll-over parameter F_2 for $\beta_{InP} = 90$ cm/GW and $\beta_{InGaAsP} = 77$ cm/GW at 1535 nm

of laser source. The first source is an 80-MHz Ti:sapphire-pumped commercial optical parametric oscillator (Spectra Physics OPAL) operating at 1535 nm, with a spectral bandwidth ($\Delta\lambda$) of 15 nm and a pulse duration of 190 fs. The second source is a home-built 60-MHz Er:Yb:glass laser operating at the same center wavelength with 20-ps ($\Delta\lambda < 1$ nm) or 3.12-ps ($\Delta\lambda = 1.8$ nm) pulse duration, depending on the SESAM used in the laser cavity.

Figure 4 shows the measured nonlinear reflectivities (dots) with the three different pulse durations of the laser sources. As expected, the strength of the roll-over increases with decreasing pulse duration (see Table 1). For the fs-pulse-duration measurements, the roll-over is so strong that neither the saturation fluence nor the modulation depth can be measured.

The TPA coefficient of InGaAsP was calculated from the theory of [18] to be $\beta_{InGaAsP} = 77$ cm/GW; this value has been experimentally verified in [19]. A direct estimation for InP from theory [18] gives $\beta_{InP} = 30$ cm/GW at 1535 nm. However, different experimental values for β_{InP} have been published, from 24 to 1800 cm/GW [20–22]. Here we choose the value of β_{InP} from [21], which has been used for previous papers on TPA in SESAMs [23]. Note that this value of $\beta_{InP} = 90$ cm/GW was measured for a wavelength of 1064 nm; according to the scaling rule of Van Stryland [18] for InP, β should be 16% smaller at 1535 nm. Even when using the largest reasonable value from the literature (90 cm/GW), we still obtain less induced absorption than experimentally observed for picosecond pulses (Table 1 and Fig. 4).

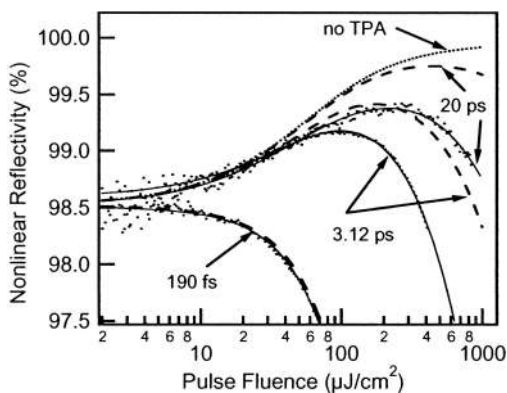The simulated nonlinear reflectivity almost perfectly fits the data obtained with the 190-fs pulses. However, for the longer pulse durations of 3.1 ps and 20 ps, the measured F_2 values are smaller than calculated by factors of 2.6 and 4.5 times, respectively (compare the measured and calculated values in Table 1).

In Fig. 5, we compare the F_2 values for both the measured and the calculated (using (8)) inverse saturable absorption as a function of the pulse duration. Even though literature values for TPA coefficients differ quite significantly [18–22], as indicated by the factor-2 error bars in Fig. 5, the difference between the measured data and the expectations for a pure TPA effect is significant. Recall that the reflectivity decreases with increasing pulse fluence as expected for a second-order process (and thus can be described by a constant F_2). Most surprisingly, the dependence of F_2 on the pulse duration is not as expected. This is clearly seen in the slope of 0.6 instead of 1.0 in the log–log plot in Fig. 5. This suggests that the roll-over is not only resulting from an instantaneous second-order process, such as TPA. The physical origin of this additional induced absorption is not clear yet. Possible mechanisms include free-carrier absorption (possibly with TPA-generated carriers), Auger recombination, hot-carrier generation, and lattice heating.

For practical applications it is important to note that for a given pulse duration, the induced absorption coefficient is proportional to the incident intensity (as for TPA) and can be well described by a F_2 value for absorptions up to some percent. However, while for TPA the factor F_2 scales linearly with the pulse duration, this dependence is significantly weaker for the additional effect (compare (8) and Fig. 5). Consequently, F_2 has to be measured at the target pulse duration. Figure 5 also displays the data for the coated SESAM. The dependence of the roll-over on the pulse duration is the same as for the uncoated SESAM.

4 Effects of the roll-over for passive mode locking of lasers

Whatever the physical origin of the additional induced absorption may be, the effect is technologically important. In this section we discuss its importance for the performance of passively mode-locked lasers.

4.1 Reduced modulation depth, increased nonsaturable losses

It is obvious (see Fig. 2) that the roll-over reduces the effective modulation depth and increases the effective nonsaturable losses, which add to the cavity losses and reduce the output power. Moreover, the reduced effective modulation
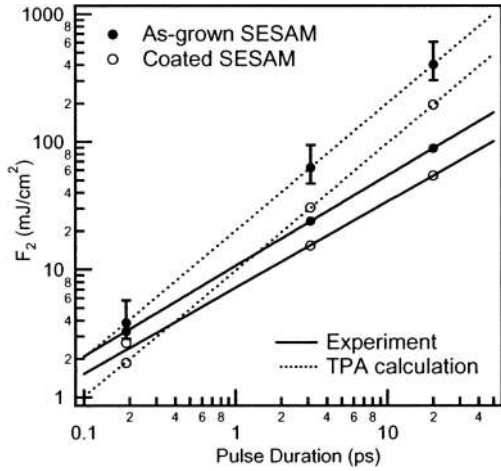

FIGURE 4 Nonlinear reflectivity vs. pulse fluence of the as-grown AlGaAsSb SESAM with three different pulse durations. *Dots*: measured data, *solid lines*: fits with induced absorption model, *dashed lines*: calculated curves for TPA only, and *dotted line*: without TPA

FIGURE 5 Comparison of the dependence of F_2 coefficients on pulse duration for both the pure TPA simulation and the measured data for the as-grown and the coated SESAMs

depth reduces the strength of the pulse shaping and in this way can lead to the generation of longer pulses or an increased susceptibility to destabilizing influences (as e.g. sensitivity to feedback). Finally, a strong roll-over can induce a tendency for the generation of multiple pulses, since these may then have lower losses at the SESAM due to their reduced energies.

These detrimental effects are most critical for short pulses, where the roll-over is the strongest, and in situations where the modulation depth is made small (e.g. through the choice of a rather thin absorber layer), so that the induced absorption gains relative importance. The latter situation is most likely for lasers which are optimized either for very high output powers or for very high (multi-GHz) pulse-repetition rates, because both design goals tend to increase the tendency for Q-switching instabilities and thus often demand the use of SESAMs with small modulation depth.

4.2 *Effect of roll-over on QML threshold*

An inverse saturable absorption reduces the tendency for Q-switched mode locking (QML) [14]. This is not only due to the reduced effective modulation depth, but also (and more importantly) due to the reduced slope of the nonlinear reflectivity curve. In this section we show quantitatively how an induced nonlinear absorption in a SESAM lowers the threshold power for stable mode locking without Q-switching instabilities.

According to the derivation of (7), we obtain the loss q_p for the pulse averaged over the whole temporal pulse profile by replacing the fluence F_p with E_p/A_A and F_{sat} with E_{sat}/A_A, where E are the energies and A_A is the mode area on the SESAM (the index A is used for properties of the absorber whereas L is related to properties of the gain medium). For small modulations ($q_0 \ll 1$) and with negligible nonsaturable losses, we can replace the maximum reflectivity change ΔR in (7) by $\Delta R = 1 - \exp(-q_0) \approx q_0$, leading to

$$q_p(E_p) = q_0(1 - \exp(-E_p/E_{sat,A}))\frac{E_{sat,A}}{E_p} + \frac{E_p}{A_A F_2} . \quad (16)$$

Now we consider the stability of a mode-locked laser against QML with the saturation energy $E_{sat,L}$ and the upper-state lifetime τ_L of the gain medium. The dynamical variables are the intracavity average power $P = E_p/T_R$ (with the cavity round-trip time T_R) and the gain coefficient g. We use the results of [9, 24], where it was found that the steady-state solution for P and g is stable if

$$\frac{1}{\tau_L} + \frac{P}{E_{sat,L}} > -P\frac{\partial q_p}{\partial E_p} . \quad (17)$$

Here, the right-hand side describes the destabilizing effect that the saturable absorber typically favors increased pulse energies by reducing its loss ($\partial q_p/\partial E_p < 0$). On the left-hand side, the second term is usually dominating for operation well above threshold, and it describes the stabilizing effect of gain saturation. Stability against Q-switching is achieved when the stabilizing effect of gain saturation is stronger than the destabilizing effect of the absorber.

In the approximation for strong saturation ($E_p \geq 2E_{sat,A}$), (16) simplifies to

$$q_p(E_p) = q_0\frac{E_{sat,A}}{E_p} + \frac{E_p}{A_A F_2} , \quad (18)$$

and we obtain

$$\frac{\partial q_p}{\partial E_p} = -q_0\frac{E_{sat,A}}{E_p^2} + \frac{1}{A_A F_2} , \quad (19)$$

which leads to the stability condition

$$\frac{1}{\tau_L} + \frac{P}{E_{sat,L}} > P\left(q_0\frac{E_{sat,A}}{E_p^2} - \frac{1}{A_A F_2}\right) , \quad (20)$$

or well above threshold to the condition [5, 14]

$$E_p^2 > \frac{E_{sat,A}\Delta R}{\frac{1}{E_{sat,L}} + \frac{1}{A_A F_2}} . \quad (21)$$

For $F_2 \to \infty$ (i.e. without induced nonlinear losses) we retrieve the simpler equation [5]

$$E_p^2 > E_{sat,A} E_{sat,L}\Delta R . \quad (22)$$

With finite F_2, the threshold for stable mode locking (called the QML threshold) is reduced, and for small enough values of F_2 the saturation energy $E_{sat,L}$ of the gain medium is no longer important. This is because $|\partial q_p/\partial E_p|$ gets very small, so that the destabilizing effect of the absorber is effectively removed by the inverse saturable absorption, and gain saturation is no longer needed to stabilize the laser. In this regime, minimization of the mode size in the gain medium, which leads to a minimized value of $E_{sat,L}$, is no longer necessary for stable operation. Indeed, we found experimentally that two different 10-GHz Er:Yb:glass lasers, which used the same SESAM but very different mode areas in the gain media, exhibited quite similar QML thresholds.

Note that it is often convenient to rewrite (21) as

$$E_p > \frac{1}{\frac{1}{E_{sat,L}} + \frac{1}{A_A F_2}}\frac{\Delta R}{S} , \quad (23)$$

which contains only measurable SESAM parameters, with the saturation parameter $S = E_p/E_{sat,A}$ of the absorber. For designing lasers, it is often convenient to fix a certain value of S for the desired output power, and this value of S can later be achieved by adjusting the mode size on the absorber. For comparison, the use of (21) could lead to designs with unrealistic values of S – e.g. to too high values that can lead to overheating or even damage of the absorber. Typical values of S vary between 2 and 10, and values around 4 lead to the shortest pulses for lasers without soliton pulse shaping [25].

5   Optimization of the roll-over for applications

As we have seen that the roll-over in nonlinear reflectivity curves of SESAMs has important consequences for mode-locked lasers, it is interesting to discuss how we can optimize the strength of the roll-over for particular applications. Design guidelines are obtained from (8), (11), (12), and (15) and from the results of Sect. 3. Recall that for picosecond operations the actual roll-over parameter F_2 cannot be calculated from TPA but should be measured.

Different top coatings can increase or decrease the field intensity in the device, changing the field enhancement in the absorber [15]. The modulation depth ΔR and the nonsaturable losses ΔR_{ns} scale proportionally and the saturation fluence F_{sat} inversely proportionally with the normalized field $|E_n|^2$. The roll-over parameter F_2 scales inversely quadratically with $|E_n|^2$. This has been verified experimentally; see Table 2. All experimental values are in reasonable agreement with the calculated $|E_n|^2$-ratio of 1.32. Consequently, the saturation curve is rescaled but not changed in shape. For example, the saturation parameter S_0, for which the maximum reflectivity is reached, stays unchanged. Therefore, in order to modify the relative strength of saturable absorption and the roll-over, one has to redesign the SESAM.

For now we consider only TPA. In the case of InP, it has been demonstrated that increasing the thickness of the spacer layer results in stronger TPA [14]. A different possibility to enhance the roll-over relative to the saturable absorption is shifting from an anti-resonant to a resonant design [2, 26, 27] and placing the saturable absorber away from the field maximum.

In some cases one may want to reduce the TPA effect. As TPA occurs mostly in the spacer layer and the first DBR pairs, the choice of the materials in this region can change the roll-over. In the InGaAsP/InP system, the β coefficients are finite for high- and low-index Bragg layers ($\beta_{InGaAsP} = 77$ cm/GW and $\beta_{InP} = 90$ cm/GW) [18, 19]. In contrast, for AlAs/GaAs Bragg mirrors, the β coefficient is negligible for AlAs and about 20 cm/GW for GaAs [18]. Consequently, it is easier to decrease induced absorption in GaAs-based SESAMs. In addition to the Bragg mirror, there is also a choice of the spacer material. We simulated a resonant SESAM design with a standard 30-pair AlAs/GaAs DBR. The $\lambda/4$ spacer layer between DBR and absorber is either AlAs or GaAs or a combination of both (see the design in Fig. 6). We start with an AlAs or GaAs layer thinner than $\lambda/4$ and complete the $\lambda/4$ spacer with the other material. Figure 7 displays the normalized roll-over coefficient F_2 vs. the AlAs or GaAs spacer-layer thickness (left-hand axis) as well as the field enhancement in the absorber (right-hand axis). According to the simulation, we can decrease the strength of TPA by a factor of more than 2.5 by replacing GaAs with TPA-free AlAs. There is no significant difference whether GaAs or AlAs is close to the absorber and the field-enhancement factor stays almost constant under those design modifications. This has been experimentally verified by growth of two SESAMs differing only by their spacer layers: $F_{2,GaAs} = 60.5$ mJ/cm^2, $F_{2,AlAs} = 129.4$ mJ/cm^2 and $|E_{n,GaAs}|^2 = 3.77$, $|E_{n,AlAs}|^2 = 3.69$ in the absorber. Experimentally we obtain 2.1 times weaker roll-over by using the AlAs spacer layer instead of GaAs. In Fig. 8, we show the impact of a factor of only 2.5 in F_2 between GaAs and AlAs spacers on the nonlinear reflectivity curves. For short pulses, the nonlinear reflectivity curve with a GaAs spacer shows no modulation at all, see e.g. Fig. 4, but with the AlAs spacer a finite modulation depth becomes available. Even for longer pulses with S_0 in the range of 5–10, the difference between GaAs and AlAs spacers is evident.
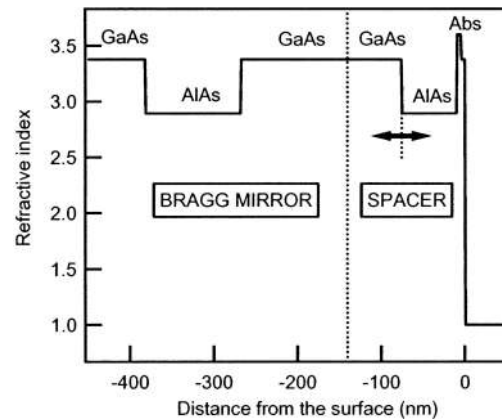

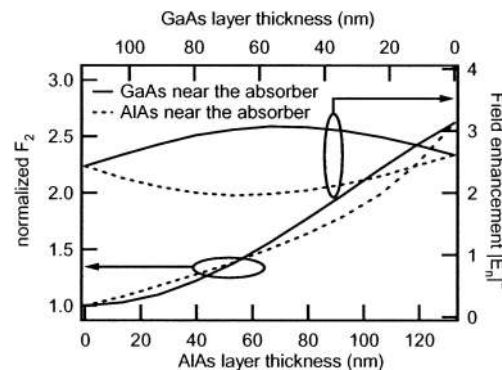**FIGURE 6**   Spacer layer modification with AlAs or GaAs material

FIGURE 7   Simulation of the F_2 parameter by changing the composition of the spacer layer from GaAs to AlAs and the corresponding field enhancement factor in the absorber. *Solid line*: GaAs near the absorber, *dashed line*: AlAs near the absorber

Pulse duration	$\dfrac{F_{sat,as\text{-}grown}}{F_{sat,coated}}$	$\dfrac{\Delta R_{coated}}{\Delta R_{as\text{-}grown}}$	$\sqrt{\dfrac{F_{2,as\text{-}grown}}{F_{2,coated}}}$
20 ps	1.38	1.34	1.28
3.1 ps	1.76	1.39	1.25

TABLE 2   Ratios of measured parameters for as-grown and coated SESAMs. $|E_n|^2_{coated}/|E_n|^2_{as\text{-}grownd} = 1.32$ (calculated)

A further reduction of TPA can be obtained by reducing the penetration depth into the Bragg mirror. One approach would be to use materials with higher index contrast, like CaF_2/GaAs [28, 29] or oxidized GaAs/AlAs mirrors [30, 31]. For wavelengths above 1500 nm, TPA in the DBR can be easily reduced by replacing the high-index layer GaAs by $Al_xGa_{1-x}As$ without reducing the mirror bandwidth significantly. Only small amounts of aluminum are needed, reaching TPA-free material (for $\lambda > 1500$ nm) at a 20% aluminum concentration. Summarizing, it is generally easier to increase the strength of TPA, while a reduction of TPA is more challenging and may require changing Bragg and spacer-layer materials.

One may also consider ways to modify the strength of the additional TPA-like effect, which we observed for picosecond pulses. At this time it is not clear what the origin of this effect is. We observed this effect in SESAMs with different absorber materials on AlAs/GaAs and InP/InGaAsP Bragg mirrors. It is not known so far how the strength of this effect depends on the material composition and wavelength; this needs further investigation. Note that minimization of the roll-over will normally not be required in the picosecond regime (as it tends to be weak naturally), while maximization may well be desirable for the suppression of Q-switching instabilities.

6   Conclusions

We have investigated in detail the roll-over of nonlinear reflectivity curves of various SESAMs. While for femtosecond pulses the observed roll-over is in good agreement with expectations for two-photon absorption (TPA), there appears to be an additional inverse saturable absorption effect for picosecond pulses, where the roll-over is weaker than for femtosecond pulses but definitely stronger than expected from TPA alone. While the physical origin of this additional induced nonlinear absorption remains to be clarified, important technological consequences are already apparent. In particular, the roll-over can greatly help to suppress Q-switching instabilities in passively mode-locked picosecond lasers operated with multi-GHz pulse-repetition rates. With strong enough (but not excessive) saturation on the

SESAM, Q-switching instabilities can be fully eliminated without minimization of the mode size in the gain medium. The discovered stronger roll-over allows us to reach this goal in the picosecond regime, where TPA alone would normally be much too weak. This finding explains why the QML thresholds of several lasers with high repetition rates have recently been found to be significantly lower than expected.

We also discussed ways to influence the strength of the roll-over via the SESAM design. Significant changes have been demonstrated by modification of the spacer layers around the absorber layer. The choice of Bragg-layer materials is also of great importance, although the material dependence of the picosecond roll-over remains to be investigated in detail.

REFERENCES

1 U. Keller, D.A.B. Miller, G.D. Boyd, T.H. Chiu, J.F. Ferguson, M.T. Asom: Opt. Lett. **17**, 505 (1992)
2 U. Keller, K.J. Weingarten, F.X. Kärtner, D. Kopf, B. Braun, I.D. Jung, R. Fluck, C. Hönninger, N. Matuschek, J. Aus der Au: IEEE J. Sel. Top. Quantum Electron. **2**, 435 (1996)
3 U. Keller: Nature **424**, 831 (2003)
4 U. Keller: Prog. Opt. **46**, 1 (2004)
5 C. Hönninger, R. Paschotta, F. Morier-Genoud, M. Moser, U. Keller: J. Opt. Soc. Am. B **16**, 46 (1999)
6 S.C. Zeller, L. Krainer, G.J. Spühler, R. Paschotta, M. Golling, D. Ebling, K.J. Weingarten, U. Keller: Electron. Lett. **40**, 875 (2004)
7 R. Paschotta, L. Krainer, S. Lecomte, G.J. Spühler, S.C. Zeller, A. Aschwanden, D. Lorenser, H.J. Unold, K.J. Weingarten, U. Keller: New J. Phys. (2004) to appear
8 E. Innerhofer, T. Südmeyer, F. Brunner, R. Häring, A. Aschwanden, R. Paschotta, U. Keller, C. Hönninger, M. Kumkar: Opt. Lett. **28**, 367 (2003)
9 A. Schlatter, S.C. Zeller, R. Grange, R. Paschotta, U. Keller: J. Opt. Soc. Am. B **21**, 1469 (2004)
10 A.C. Walker, A.K. Kar, W. Ji, U. Keller, S.D. Smith: Appl. Phys. Lett. **48**, 683 (1986)
11 D.J. Harter, Y.B. Band, E.I. Ippen: IEEE J. Quantum Electron. **QE-21**, 1219 (1985)
12 E.R. Thoen, E.M. Koontz, M. Joschko, P. Langlois, T.R. Schibli, F.X. Kärtner, E.P. Ippen, L.A. Kolodziejski: Appl. Phys. Lett. **74**, 3927 (1999)
13 M. Haiml, R. Grange, U. Keller: Appl. Phys. B **79**, 331 (2004)
14 T.R. Schibli, E.R. Thoen, F.X. Kärtner, E.P. Ippen: Appl. Phys. B **70**, S41 (2000)
15 L.R. Brovelli, U. Keller, T.H. Chiu: J. Opt. Soc. Am. B **12**, 311 (1995)
16 O. Ostinelli, G. Almuneau, M. Ebnöther, E. Gini, M. Haiml, W. Bächtold: Electron. Lett. **40**, 940 (2004)
17 R. Grange, O. Ostinelli, M. Haiml, L. Krainer, G.J. Spühler, S. Schön, M. Ebnöther, E. Gini, U. Keller: Electron. Lett. (2004)
18 E.W. Van Stryland, M.A. Woodall, H. Vanherzeele, M.J. Soileau: Opt. Lett. **10**, 490 (1985)
19 H.K. Tsang, R.V. Penty, I.H. White, R.S. Grant, W. Sibbett, J.D. Soole, H.P. LeBlanc, N.C. Andreadakis, R. Bhat, M.A. Koza: J. Appl. Phys. **70**, 3992 (1991)
20 D. Vignaud, J.F. Lampin, F. Mollot: Appl. Phys. Lett. **85**, 239 (2004)
21 M.D. Dvorak, B.L. Justus: Opt. Commun. **114**, 147 (1995)
22 R.A. Bendorius, E.K. Maldutis: Sov. Phys. Coll. **23**, 69 (1983)
23 E.R. Thoen, E.M. Koontz, D.J. Jones, D. Barbier, F.X. Kärtner, E.P. Ippen, L.A. Kolodziejski: IEEE Photon. Technol. Lett. **12**, 149 (2000)
24 H.A. Haus: IEEE J. Quantum Electron. **QE-12**, 169 (1976)
25 R. Paschotta, U. Keller: Appl. Phys. B **73**, 653 (2001)
26 V. Liverini, S. Schön, R. Grange, M. Haiml, S.C. Zeller, U. Keller: Appl. Phys. Lett. **84**, 4002 (2004)
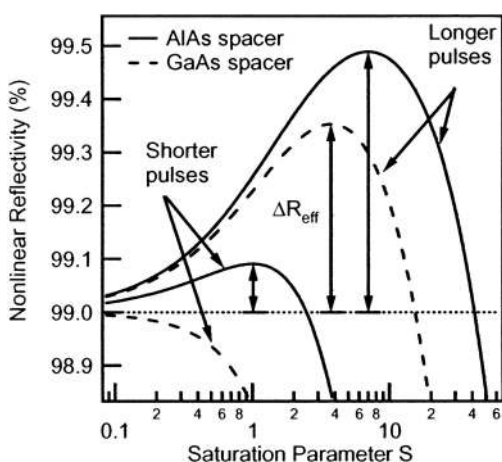

FIGURE 8 Calculated nonlinear reflectivity vs. saturation parameter for short and long pulses with a spacer layer composed of GaAs or AlAs

27 K.J. Weingarten, G.J. Spühler, U. Keller, L. Krainer: US Patent No. 6 538 298 (2003)

28 Z. Shi, H. Zogg, P. Müller, I.D. Jung, U. Keller: Appl. Phys. Lett. **69**, 3474 (1996)

29 S. Schön, M. Haiml, L. Gallmann, U. Keller: Opt. Lett. **27**, 1845 (2002)

30 D.E. Wohlert, H.C. Lin, K.L. Chang, G.W. Pickrell, J.J.H. Epple, K.C. Hsieh, K.Y. Cheng: Appl. Phys. Lett. **75**, 1371 (1999)

31 D.J. Ripin, J.T. Gopinath, H.M. Shen, A.A. Erchak, G.S. Petrich, L.A. Kolodziejski, F.X. Kärtner, E.P. Ippen: Opt. Commun. **214**, 285 (2002)